

Application of a Virtual-Boundary Method for the Numerical Study of Oscillations Developing Behind a Cylinder Near A Plane Wall

E. Kit, N. V. Nikitin, V. M. Shmidt, and A. Yakhont

Received March 26, 2003

Abstract — The conditions of onset and the character of the oscillations developing behind a circular cylinder located above a plane wall (screen) in a flow with a velocity profile of the boundary layer type are studied numerically. The dependence of the critical Reynolds number (at which a steady flow regime in the wake behind the cylinder is replaced by an oscillatory regime) on the cylinder-wall gap and the free-stream boundary layer thickness is found.

Keywords: two-dimensional Navier-Stokes equations, finite-element method, unsteady flow, critical Reynolds number, Strouhal number

The presence of a plane wall in a crosswise flow past a cylindrical obstacle (Fig. 1) significantly affects the flow pattern. This is attributable to three main factors. First, the no-flow conditions on the wall prevent the expansion of the flow. This results in the appearance of a finite lift force exerted on the obstacle and directed away from the wall. Second, the free-stream velocity profile is nonuniform. The presence of a velocity shear produces an asymmetric action on the cylinder. Third, the no-slip conditions on the wall distort the flow in the wake behind the cylinder and change the flow stability conditions.

Due to its practical importance, the flow past a circular cylinder near a plane wall has been studied experimentally in a number of papers (see [1, 2]). Most of the experiments were performed at high Reynolds numbers $Re = 10^4$ – 10^6 , important for the design of ground structures. It has been established that the presence of a wall damps vortex shedding from the cylinder. For the critical cylinder-wall gap, at which oscillations with a fixed frequency in the wake are suppressed, values ranging between 0.125 and 0.9 were obtained in different experiments (in all the experiments, the linear scale was the cylinder diameter). This large scatter is attributable to the different experimental conditions, such as the free-stream turbulence rate, the boundary layer thickness at the cylinder location, etc.

The flow past a cylinder near a wall at low Reynolds numbers ($Re \sim 10^2$) considered in this study is of interest from both the fundamental and the practical point of view. An example of such a flow is the flow past underwater pipelines at depths of several tens of meters, i.e. beyond the coastal surf zone [3]. To the authors' knowledge, there has been only one experiment [4] on this range of Reynolds numbers ($Re = 170$), in which a two-row Karman vortex street was observed behind the cylinder for a gap $s = 0.6$ and a one-row street for $s = 0.1$. However, study [4] dealt with the motion of a cylinder in a stationary fluid and hence the effects associated with the free-stream velocity profile were not considered.

In [5], the flow past a cylinder in a flat-plate boundary layer was studied numerically over the range $Re = 80$ – 1000 (Reynolds number based on the velocity at infinity and the diameter of the cylinder). In all the calculations, the center of the cylinder was located at a distance of 16 from the leading edge of the plate. Thus, the boundary layer thickness at the cylinder location was uniquely related with the Reynolds number. The dependence of the critical Reynolds number Re^* on the gap was calculated. For $s < 0.2$, no oscillations were observed behind the cylinder up to $Re = 1000$. A similar result was obtained in [6], in which the flow past a cylinder in a plane channel at $Re < 300$ was considered. For a Poiseuille

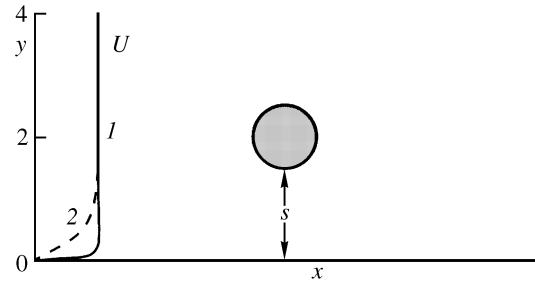


Fig. 1. Flow diagram and free-stream velocity profiles; 1 — thin boundary layer, 2 — thick boundary layer

free-stream velocity profile, vortex shedding was suppressed as the cylinder approached to within $s = 0.25$ of the channel walls. We note that in these studies, the dependence of the results, in particular the function $Re^*(s)$, on the free-stream velocity profile was not investigated.

Our aim was to study numerically the influence of the free-stream velocity profile $U(y)$ on the stability of the flow past a cylinder near a plane wall. For this purpose, we calculated the critical Reynolds numbers $Re^*(s)$ for velocity profiles of the boundary layer type $U(y) = th(y/d)$ at two values of the parameter d characterizing the boundary layer thickness. It was shown that the free-stream boundary layer thickness is very important.

In [5], a finite-difference method of calculation on a nonorthogonal grid adapted to the cylinder and wall boundaries was used. In [6], a finite element method was employed. Both these numerical methods make it possible to concentrate the grid points near the obstacle and to satisfy exactly the boundary conditions on the rigid boundaries. However, the complex grid noticeably reduces the effectiveness of the algorithm. In particular, for solving elliptic problems (for finding the stream function in terms of the vorticity or for calculating the pressure) it is necessary to use iteration procedures.

In this study, we used an alternative approach, namely, a virtual-boundary method. In this method, the Navier-Stokes equations are solved in a rectangular domain on a simple orthogonal grid. Obstacles of an arbitrarily complex shape, present in the flow domain, are modeled in the equations by introducing artificial forces specially distributed to ensure zero velocities (for no-slip conditions) on given surfaces (virtual boundaries) inside the flow region. The advantages of this approach as compared with methods using adaptive grids are: a significant simplification of the computer programs, the simplicity of grid generation (even for moving obstacles), a noticeable reduction in the memory required, and the speeding up of the algorithms. In particular, elliptic problems can be solved by fast direct (iterationless) methods. Since in general the obstacle boundaries do not pass through the grid points, the formulation of the boundary conditions requires the use of interpolation methods. The method of velocity interpolation at the boundary points using the values at the grid points and the method of introducing the artificial forces determine the specific variant of the virtual-boundary method.

In this study, we will use a variant similar to that developed in [7]. This method differs from the other analogous methods reviewed in [7] in having greater interpolation stability and, what is most important, in applying the artificial forces only at grid points located inside or on the boundary of the obstacles. Thus, the method does not introduce any nonphysical disturbances into the flow domain. An other feature of the method [7] is the introduction of mass sources (sinks) (with zero integral intensity) inside the obstacles, which significantly increases the solution accuracy.

1. FORMULATION OF THE PROBLEM AND METHOD OF SOLUTION

We will consider a plane flow of viscous incompressible fluid in a rectangular domain

$$(x, y) \in \{0 \leq x \leq X_m, 0 \leq y \leq Y_m\}$$

with a circular obstacle (cylinder) whose center is located at the point (x_c, y_c) . In the section $x = 0$ (the inlet section), a velocity distribution $\mathbf{v} = (U(y), 0)$ is specified (Fig. 1). The flow is described by the unsteady

2D Navier-Stokes equations

$$\frac{\partial \mathbf{v}}{\partial t} = -(\mathbf{v}\nabla)\mathbf{v} + \frac{1}{\text{Re}}\nabla^2\mathbf{v} - \nabla p + \mathbf{F} \quad (1.1)$$

$$\nabla \cdot \mathbf{v} = 0 \quad (1.2)$$

Here, $\mathbf{v} = (u, v)$ is the velocity field, p is the kinematic pressure, t is time, and Re is the Reynolds number. The length and velocity scales are the diameter of the cylinder and the maximum velocity in the inlet section. On the bottom wall ($y = 0$) and on the obstacle surface, the no-slip conditions are specified, while on the top boundary ($y = Y_m$) the free-slip condition is assumed to apply. In the outlet section, assumed to be located fairly far away from the obstacle, soft boundary conditions $\partial^2 u / \partial x^2 = \partial v / \partial x = 0$ are specified.

We introduce the artificial force $\mathbf{F} = (-U''(y)/\text{Re}, 0)$ on the right side of Eq. (1.1) to satisfy the condition that, in the absence of an obstacle, the velocity field $\mathbf{v} = (U(y), 0)$ is the solution over the entire flow region. Thus, we eliminate the dependence of the free-stream velocity profile on the Reynolds number and the distance from the inlet section. In this study, we use a $U(y)$ of the boundary-layer type:

$$U(y) = \text{th} \frac{y}{d} \quad (1.3)$$

The parameter d characterizing the boundary layer thickness is related with the boundary layer displacement thickness δ and the momentum thickness θ by the formulas

$$\delta = d \ln 2, \quad \theta = d(1 - \ln 2)$$

To eliminate the problem of initial conditions, the solution was obtained from the state of rest $\mathbf{v}(t = 0) = 0$. The flow was accelerated on the initial time interval $\tau \sim 1$ by smooth variation of the inlet boundary conditions:

$$\begin{aligned} \mathbf{v}(x = 0) &= f(t)(U(y), 0), & f(0) &= 0, & f(t \geq \tau) &= 1 \\ f'(0) &= f''(0) = f'(\tau) = f''(\tau) = 0 \end{aligned}$$

In the process of varying the Reynolds number (without changing the geometric and grid parameters), the initial data were taken from the calculation results for nearby values of Re .

For the numerical solution of the problem, we used a virtual-boundary method similar to [7]. The differences with respect to the original variant consisted in the time integration scheme and a slight change in the interpolation procedure, which increased its stability. The problem in the spatial variables was discretized using a second-order standard finite-difference method on staggered grids [8]. In accordance with the staggered-grid principle, the pressure is found at the grid points lying at the centers of the calculation cells, and the velocity components at grid points displaced by a half-step in the direction of the velocity component considered. Various details of the derivation and the properties of the finite-difference equations can be found in [9–11]. As in [7], the time integration was performed using a semi-implicit scheme based on a third-order Runge-Kutta method. However, instead of the scheme [12] used in [7], in this study we employed a scheme designed in [13], which uses the same computer memory but makes it possible to estimate the local error easily and efficiently and to control automatically the integration step [14].

In calculating the pressure on a grid nonuniform in both directions, the Poisson equation was solved using a fast direct cyclic-reduction method [15].

2. CYLINDER IN A UNIFORM FLOW IN THE ABSENCE OF A WALL

To study the potential and properties of the numerical procedure and to determine the algorithm parameter values, we performed comprehensive numerical investigations of the flow past a cylinder in the absence of a wall. In these calculations, the inlet flow was uniform and on both the top and bottom boundaries the

Table 1

Re	X_m, Y_m, X_c	$I_m \times J_m$	$I_c \times J_c$	C_x	C'_y	St	References
40	50, 30, 15	128×96	16×16	1.57	–	–	–
40	50, 30, 15	256×192	32×32	1.57	–	–	–
40	50, 30, 15	512×384	64×64	1.56	–	–	–
40	100, 60, 30	256×192	16×16	1.53	–	–	–
100	50, 30, 15	256×192	32×32	1.365	0.33	0.167	–
200	50, 30, 15	256×192	32×32	1.36	0.68	0.199	–
200	50, 30, 15	512×384	64×64	1.35	0.68	0.198	–
200	100, 60, 30	512×384	32×32	1.34	0.66	0.196	–
40	–	–	–	1.51	–	–	[7]
40	–	–	–	1.51	–	–	[16]
100	–	–	–	1.33	0.32	0.165	[7]
100	–	–	–	1.33	0.33	0.165	[16]

free-slip condition was specified. Along with the Reynolds number, we varied the calculation domain dimensions X_m and Y_m , the distance from the inlet section to the cylinder center X_c , and the grid point number $I_m \times J_m$. In each direction the grid points were concentrated towards the center of the cylinder. The degree of concentration was specified by the number of grid points $I_c \times J_c$ contained in a square circumscribing the cylinder. The calculations were performed on the range of Reynolds numbers from 10 to 200, on which, according to the available experimental data, the flow is still two-dimensional.

Some calculation results are presented in Table 1, which contains the values of the drag coefficient C_x , the oscillation amplitude of the lift force coefficient C'_y , and the Strouhal number St. The dependence of the results on the calculation domain and the grid parameters is illustrated for $Re = 40$ and 200. Over the entire range of Reynolds numbers considered, a 256×192 grid with $X_m = 50$ and $Y_m = 30$ ensures satisfactory results. Most of the results presented below were obtained for these values of the parameters. In addition to our results, for comparison in Table 1 we present the calculation results [7, 16] for $Re = 40$ and 100. The differences in the drag coefficient amount to 3–4% and, in C'_y and St, to less than 1%. We note that the numerical and experimental results published in the literature have a much greater scatter.

The drag law $C_x(Re)$ obtained is presented in Fig. 2. Figure 3 shows the dependences $C'_y(Re)$ and $St(Re)$ for the oscillatory regimes, observed starting from $Re = Re^* = 46$. All the results presented, including the critical Reynolds number, lie within the scatter of the available literature data.

In the steady regimes, a recirculating flow in the form of two counter-rotating eddies develops behind the cylinder (Fig. 4, $Re = 40$). The length of this recirculating flow region L_b as a function of Re shown in Fig. 5 agrees well with the experimental dependence $L_b = 0.065(Re - 7)$ [17].

The flow structure in the unsteady regimes is shown in Fig. 6, in which the instantaneous vorticity fields $\omega = \partial v / \partial x - \partial u / \partial y$ are plotted for two Reynolds numbers $Re = 50$ and 200. The dark and light regions in the figures correspond to negative and positive values of ω , respectively. The distributions of ω reflect the presence of a two-row Karman vortex street behind the cylinder.

3. THE FLOW BEHIND THE CYLINDER IN THE PRESENCE OF A WALL

The calculations were performed for two values of the parameter d characterizing the free-stream boundary layer thickness (1.3): $d = 0.1$ (thin boundary layer) and 0.5 (thick boundary layer). These values correspond to the range considered in experiments [2]. The main aim of the study was to find the dependence of the critical Reynolds number of the onset of oscillations Re^* on the value of the cylinder-wall gap s . The

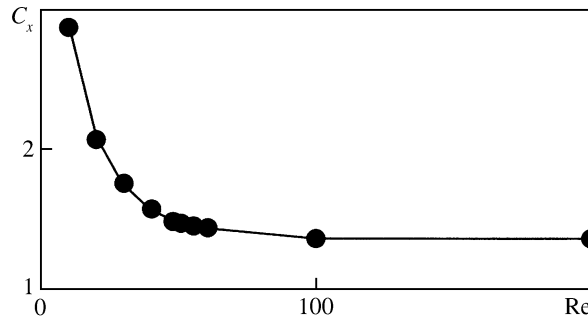
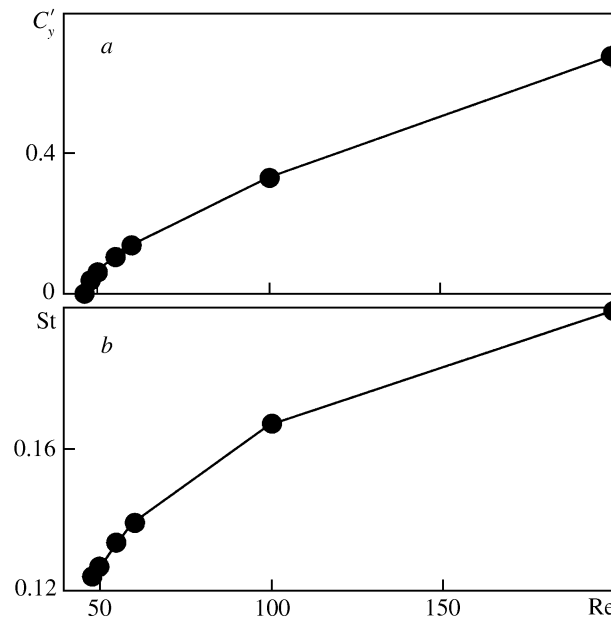


Fig. 2. The cylinder drag law

Fig. 3. The lift-force coefficient oscillation amplitude (*a*) and the Strouhal number (*b*) in the flow past a cylinder

dimensions of the calculation domain and the values of the other algorithm parameters were determined from the results of methodological calculations for an unbounded region.

In varying the Reynolds number to determine its critical value at given parameters d and s , as the initial state we chose one of three variants: *a* — the state of rest with subsequent acceleration and transition to the steady-state regime; *b* — a steady flow at lower Re ; *c* — a developed unsteady flow at larger Re . At near-critical Reynolds numbers, variant *a* requires a very large calculation time due to the smallness of the disturbance amplification (attenuation) coefficient. In this respect, variant *c* is preferable. It was found that, in most cases, variant *b* gives a larger critical value Re^* than variant *c*. Thus, for the same Reynolds number we obtained both steady-state and unsteady flows. This may be attributable to the “stiff” excitation of the oscillations. We also cannot exclude the influence of numerical effects associated with specific features of the algorithm employed. To clarify this question, additional investigations, which do not enter into the scope of this study, are required.

The dependence of the critical Reynolds number Re^* on the gap s for the two free-stream velocity profiles considered, obtained for variant *c*, are presented in Fig. 7*a*. As the gap increases, in both cases $Re^*(s)$ approaches $Re^* = 46$, which corresponds to the absence of a wall. As might be anticipated, the dependence $Re^*(s)$ is stronger for the thick than for the thin boundary layer. The minimum gap for which regular periodic regimes were observed for the thick boundary layer on the range $Re \leq 500$ was $s = 0.25$. At $s = 0.2$,

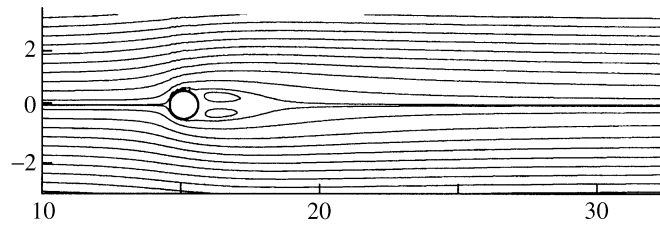
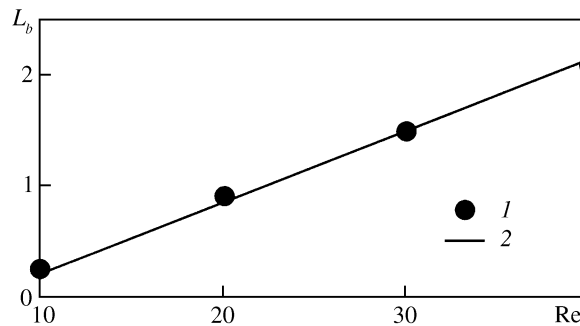
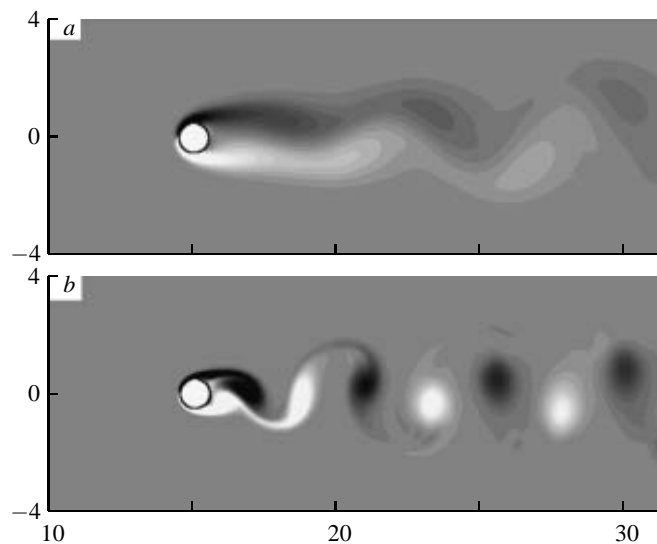
Fig. 4. Streamlines in the steady-state flow past a cylinder ($Re = 40$)

Fig. 5. The length of the recirculation-flow zone behind the cylinder: 1 — calculation, 2 — experiment [17]

Fig. 6. Instantaneous vorticity fields in the flow past a cylinder: *a* — $Re = 50$, *b* — $Re = 200$

the numerical solution approached either a steady regime or, for maximum Re , a regime of weak periodic oscillations whose period was an order of magnitude greater than that for other values of the gap. In the latter regimes, oscillations were observed only in the far wake near the outlet boundary of the calculation domain. This may be attributable to the effect of the artificial outlet conditions specified in the calculations. The complete suppression of oscillations for small gaps and a thick boundary layer agrees with the numerical calculations [5, 6] and the results of a number of experimental studies. In the case of a thin free-stream boundary layer, regular oscillations develop for all gaps, including $s = 0$, i. e. when the cylinder is in contact with the wall. In this limiting case, the critical Reynolds number is 140.

The Strouhal number St of the oscillations developed for $Re = Re^*(s)$ is given in Fig. 7*b* as a function of the gap for both values of the boundary layer thickness considered. It may be assumed that St increases

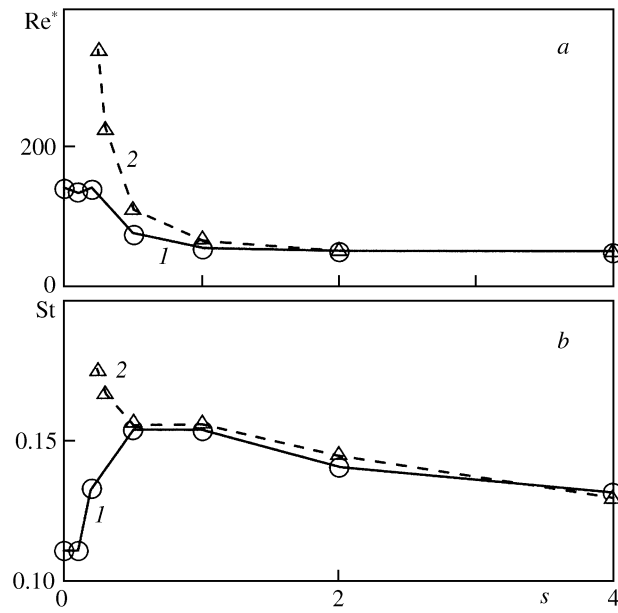


Fig. 7. Critical Reynolds number (a) and Strouhal number (b) vs. the cylinder-wall gap: 1 — $d = 0.1$, 2 — 0.5 (thin and thick boundary layers)

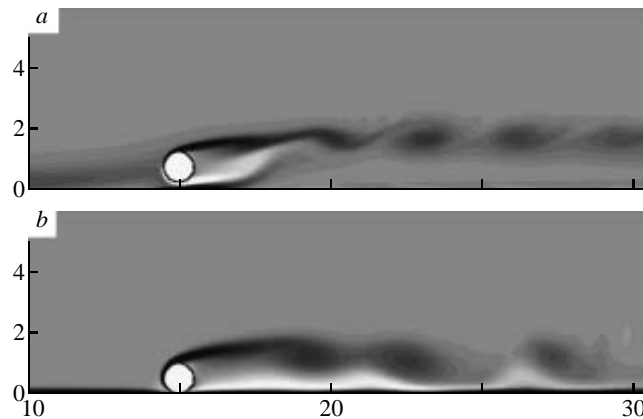


Fig. 8. Instantaneous vorticity fields: a — $d = 0.5$, $s = 0.25$, $Re = 350$, b — $d = 0.1$, $s = 0$, $Re = 140$

with increase in Re and decreases with decrease in s . In the case of a thick boundary layer, this results in the monotonous growth of the Strouhal number with decrease in the gap. For a thin boundary layer, the value of Re^* increases not so rapidly with decrease in s and the resulting behavior of $St(s)$ is nonmonotonous.

The instantaneous vorticity fields for minimum gaps and supercritical Reynolds numbers ($s = 0.25$ and 0, $Re = 350$ and 140) are shown for thick and thin boundary layers in Fig. 8. In both cases, the characteristic feature is a one-row vortex street formed in the upper part of the wake behind the cylinder. The most probable mechanism of excitation of these oscillations is Kelvin-Helmholtz instability developing in the upper flow region in the mixing layer between the outer flow and the stagnation zone behind the cylinder. With increase in the gap, the one-row structure is gradually transformed into a two-row structure and, for $s = 2$, for both values of the boundary layer thickness the vorticity fields behind the cylinder cannot be visually distinguished from that obtained in the absence of a wall (Fig. 6).

Summary. The conditions of onset and the structure of the oscillations developing in the flow past a cylinder located near a plane screen are studied numerically. Two free-stream velocity profiles are considered. It is shown that for small cylinder-wall gaps the critical Reynolds number significantly depends on the free-stream boundary layer thickness. In particular, whereas for a thick boundary layer the approach of the cylinder to the screen completely suppresses the oscillations, for a thin boundary layer it only increases the critical Reynolds number.

For small gaps, the oscillatory motion behind the cylinder is characterized by the existence of a one-row vortex street, which appears to develop as a result of the Kelvin-Helmholtz instability of the mixing layer between the outer flow and the stagnation region behind the cylinder. With increase in the gap, the flow takes the form of a two-row Karman vortex street.

The work received financial support from the Russian Foundation for Basic Research (No. 02-01-00492) and the Israel Science Foundation (grants 240/01, 150/02).

REFERENCES

1. N. M. Bychkov, N. D. Dikovskaya, and V. V. Larichkin, "Interaction of a cylinder with a nearby screen in a cross-flow," *Izv. SO Akad. Nauk SSSR, Ser. Tekhn. Nauk*, No. 1, 57–63 (1990).
2. S. J. Price, D. Summer, J. G. Smith, K. Leong, and M. P. Paidoussis, "Flow visualization around a circular cylinder near to a plane wall," *J. Fluids and Structures*, **16**, No. 2, 175–191 (2002).
3. E. Kit and M. Sladkevich, "Structure of offshore currents on Mediterranean coast of Israel," In: *6th Workshop on Phys. Processes in Natur. Waters. Ed. X. Casamitjana. Girona, Spain, 2001* (2001). pp. 97–100.
4. S. Taneda, "Experimental investigation of vortex streets," *J. Phys. Soc. Japan*, **20**, No. 9, 1714–1721 (1965).
5. C. Lei, L. Cheng, S. W. Armfeld, and K. Kavangh, "Vortex shedding suppression for flow over a circular cylinder near a plane boundary," *Ocean Engineering*, **27**, No. 10, 1109–1127 (2000).
6. L. Zovatto and G. Pedrizzetti, "Flow about a circular cylinder between parallel walls," *J. Fluid Mech.*, **440**, 1–25 (2001).
7. J. Kim, D. Kim, and H. Choi, "An immersed-boundary finite-volume method for simulations of flow in complex geometries," *J. Comput. Phys.*, **171**, No. 1, 132–150 (2001).
8. F. H. Harlow and J. E. Welch, "Numerical calculation of time-dependent viscous incompressible flow of fluid with free surface," *Phys. Fluids*, **8**, No. 12, 2182–2189 (1965).
9. G. Williams, "Numerical integration of the three-dimensional Navier-Stokes equations for incompressible flow," *J. Fluid Mech.*, **37**, Pt. 4, 727–750 (1969).
10. U. Schumann, "Subgrid scale model for finite difference simulations of turbulent flows in plane channels and annuli," *J. Comput. Phys.*, **18**, No. 4, 376–401 (1975).
11. J. Kim and P. Moin, "Application of a fractional-step method to incompressible Navier-Stokes equations," *J. Comput. Phys.*, **59**, No. 2, 308–323 (1985).
12. P. R. Spalart, R. D. Moster, and M. M. Rogers, "Spectral methods for the Navier-Stokes equations with one infinite and two periodic directions," *J. Comput. Phys.*, **96**, No. 2, 297–324 (1991).
13. N. V. Nikitin, "Statistical characteristics of wall turbulence," *Izv. Ross. Akad. Nauk, Mekh. Zhidk. Gaza*, No. 3, 32–43 (1996).
14. N. V. Nikitin, "Spectral-finite-difference method for calculating incompressible-fluid turbulent flows in tubes and channels," *Zh. Vych. Matem. i Matem. Fiz.*, **34**, No. 6, 909–925 (1994).
15. P. N. Swarztrauber, "A direct method for the discrete solution of separate elliptic equations," *SIAM J. Numer. Analysis*, **1**, No. 6, 1136–1150 (1974).
16. J. Park, K. Kwon, and H. Choi, "Numerical solutions of flow past a circular cylinder at Reynolds number up to 160," *KSME Intern. J.*, **12**, No. 6, 1200–1205 (1998).
17. S. Taneda, "Experimental investigation of the wakes behind cylinders and plates at low Reynolds numbers," *J. Phys. Soc. Japan*, **11**, No. 3, 302–307 (1956).